Analysis and Optimization of Modulation Transitions in Medium-Voltage High-Power Converters

Hector Fernandez-Rebolleda, Alain Sanchez-Ruiz, *Senior Member, IEEE*, Salvador Ceballos, Angel Perez-Basante, Juan José Valera-García, Georgios Konstantinou, *Senior Member, IEEE*, and Josep Pou, *Fellow, IEEE*

***Abstract*—Different modulation techniques need to be combined in medium-voltage high-power variable-speed drives as the fundamental output frequency changes. Due to this fact, transitions between different modulation techniques are required in a real-time converter operation. However, these transitions may generate phase overcurrent due to changes in the switching patterns. This article presents a method that analyzes and models the modulation transitions. It also identifies the optimal fundamental period angle interval where the transition should take place to minimize or eliminate any overcurrent. The proposed method is generic and can be extrapolated to any converter topology and modulation technique. It is demonstrated for transitions between selective harmonic elimination pulsewidth modulation and space vector modulation on a three-level neutral-point-clamped converter through simulations and experimentally validated in a 45-kW scaled-down converter and 6.5-MW full-scale drive.**

***Index Terms*—AC motor drives, modulation, overcurrent protection, power converter.**

I. Introduction

THE use of power converters in medium-voltage (MV) high-power (HP) applications has drastically increased due to their capabilities, such as improved output waveform quality, efficiency, reliability, and modularity [1]–[3]. To achieve an increase in voltage and power ratings, the use of multilevel converter topologies and their related modulation techniques plays an essential role [4]–[9].

Manuscript received August 21, 2020; revised December 16, 2020; accepted February 6, 2021. Date of publication February 19, 2021; date of current version June 1, 2021. This work was supported by the Basque Government within the research program ELKARTEK under the project CONVADP (KK-2020/00091). Recommended for publication by Associate Editor D. Zhang. *(Corresponding author: Hector Fernandez-Rebolleda.)*

Hector Fernandez-Rebolleda is with Ingeteam Power Technology, 48710 Zamudio, Spain (e-mail: hector.fernandez1@ingeteam.com).

Alain Sanchez-Ruiz and Juan José Valera-García are with Ingeteam R&D Europe, 48170 Zamudio, Spain (e-mail: alain.sanchez@ingeteam.com; juanjose.valera@ingeteam.com).

Salvador Ceballos and Angel Perez-Basante are with Tecnalia, Basque Research and Technology Alliance, 48160 Derio, Spain (e-mail: salvador.ceballos@tecnalia.com; angel.perez@tecnalia.com).

Georgios Konstantinou is with the School of Electrical Engineering and Telecommunications, University of New South Wales, Sydney, Sydney, NSW 2052, Australia (e-mail: g.konstantinou@unsw.edu.au).

Josep Pou is with the School of Electrical and Electronic Engineering, Nanyang Technology University, Singapore 639798, Singapore (e-mail: josep.pou@ieee.org).

Color versions of one or more of the figures in this article are available online at https://doi.org/10.1109/TPEL.2021.3060613.

Digital Object Identifier 10.1109/TPEL.2021.3060613

One of the most common MV and HP uses for multilevel converters is that of variable speed drives, typically found in different fields, such as industrial applications (pumps, fans, compressors, etc.), mining, marine propulsion, and railway traction [8]–[13]. These applications require the combination of different modulation techniques to achieve the highest available power ratings as the fundamental output frequency changes [14]–[16]. Two modulation techniques commonly used in the literature to synthesize the output voltage in variable speed drives are as follows.

1) *Space Vector Modulation (SVM) or SVM Pulsewidth Modulation (SVPWM)*: A digital implementation that controls the three-phase converter through the designed switching sequence [5], [17]–[19]. It can be applied in SVM or SVPWM variants. This modulation technique is used for low fundamental output frequencies, where the switching frequency to fundamental output frequency ratio is high.
2) *Selective Harmonic Elimination (SHE) PWM*: A precalculated modulation technique that eliminates low-order harmonics, improving voltage quality. Selective harmonic mitigation is considered as a particular case of SHE, where low-order harmonics are not completely eliminated but just mitigated [20]–[26]. SHE is used for higher output frequencies due to its synchronous characteristic, its lower switching losses, and higher voltage quality.

These modulation techniques are identified as the most common ones in medium-voltage high-power converters [14]. Due to this reason, SVM and SHE are considered in this article. On the contrary, the proposed analysis and technique can be extended to any other modulation type.

Transitions between modulation techniques may be needed in variable speed applications due to the following reasons.

1) *Output Voltage Quality*: As the fundamental output frequency increases, the switching frequency to fundamental frequency ratio of SVM decreases, which increases the harmonic distortion. Conversely, SHE generates harmonics with a frequency proportional to the fundamental output frequency; hence, as it increases, the waveform quality improves, [20], [21], [25]. Therefore, as the output frequency increases, it is preferable to move from SVM to SHE and vice versa.
2) *Thermal Limitations*: Thermal restrictions depend on the converter current and the semiconductor switching frequency [14], [27]–[30]. While SVM has a constant

switching frequency, the switching frequency of SHE increases with the output frequency and number of angles. Due to the latter one, the number of angles in an SHE pattern can be reduced as the fundamental frequency increases, thus maintaining the switching frequency below the thermal limits of the semiconductors [14], [29].

3) *Output Filter Limitation*: When an output filter is used, the employed SHE tables should be able to eliminate (or mitigate) harmonics at lower frequencies than the filter cutoff frequency to avoid possible resonances. Therefore, transitions between SHE patterns with different number of firing angles could be required as the output frequency increases/decreases.

When using different modulation techniques, the transition from one to another becomes critical as it produces a transient overcurrent that may exceed converter ratings, thus triggering the overcurrent protection.

This article proposes a technique to minimize the overcurrent produced in case of modulation transitions in variable speed drives. Owing to the proposed work in this article, any modulation technique can be combined in order to accelerate the converter up to nominal frequency. Even voltage/second strategy [31] is an approach that can be applied in classical SVM methods; this type of technique is not possible to generally be extended to any other modulation type. To the best knowledge of the authors, this is the first time that a generic modulation transition algorithm is proposed in the literature. The main contributions are as follows.

1) An analytical approach is presented to combine different modulation techniques. Dependencies of the overcurrent with different circuit parameters are analyzed.
2) An offline algorithm is proposed to minimize the overcurrent under modulation transitions. It estimates the optimum angle range where the transition between the two modulation techniques needs to take place to minimize the transient overcurrent.

The analysis has been done for a three-level converter. However, extrapolation of the methodology for any number of output voltage levels is straightforward. The inputs of the proposed analysis are: converter output voltage frequency spectrum, and load characteristics. Calculations needed to obtain these points may vary depending on both converter topology and modulation technique. Once converter output voltage is obtained, the proposed analysis is applicable for any converter topology or modulation technique. This analysis is also applicable for overcurrents in voltage source converters (VSC) or overvoltages in current source converters, whose operation is analogous. VSC case is analyzed in this article.

The rest of this article is organized as follows. Section II develops the mathematical analysis of the current transient when the modulation technique is changed. In Section III, the proposed algorithm to calculate the transient overcurrent waveform when there is a transition between modulation techniques is introduced. Besides, a study of the overcurrent dependence on the input parameters is introduced as well. Section IV presents a case study and simulation results to test the developed algorithm. In Section V, experimental results are presented for a full-scale MV drive and a voltage scaled-down testbench. Finally, Section VI concludes this article.

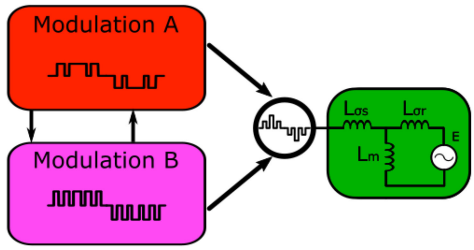

Fig. 1. Modulation transition scheme for each phase of a multiphase system.

II. Modulation Transition Analysis

To change the output voltage and frequency of an MV variable speed drive, a modulation change might be needed. To analyze this scenario, the simplified scheme illustrated in Fig. 1, where a voltage source (emulating the converter output) supplies an inductive–resistive load (i.e., asynchronous motor), is used. At a given time instant, the voltage source changes from the switching patterns provided by Modulation A to those provided by Modulation B, creating a transient in the output current.

Generally speaking, the output voltage synthesized by the initial modulation technique for a generic Phase *X* is defined as follows:

$$V_{A_X}(t) = \sum_{h=i}^{j} \left[V_{A,h} \sin\left(h\omega t + \gamma + \varphi_{A,h}\right) \right] \tag{1}$$

where $V_{A,h}$ is the amplitude of the h harmonic component of the output voltage, ω is the output frequency expressed in rad/s, t is the time in seconds, and $\varphi_{A,h}$ and $\gamma = \{0, \frac{4\pi}{3}, \frac{2\pi}{3}\}$ are the initial phase shift for the h harmonic and the phase angle component, respectively, expressed in radians. The same Fourier series expansion defines the output voltage synthesized by the switching patterns of Modulation B by just replacing $V_{A,h}$ by $V_{B,h}$ and $\varphi_{A,h}$ by $\varphi_{B,h}$.

The equivalent load impedance can be expressed as

$$Z_{n,h} = Z_h \angle\theta_h \tag{2}$$

where Z_h and θ_h are the impedance module and phase expressed in Ohms and radians, respectively, for every h harmonic [32].

The output current for Phase *X* when a transition from Modulation A to B takes place can be expressed as

$$i_X(t) = \sum_{h=i}^{j} \left[\frac{V_{B,h}}{Z_h} \sin\left(h\omega t + \gamma + \varphi_{B,h} + \theta_h\right) \right] + R_X(T_0)\, e^{-t\frac{R_{\text{load}}}{L_{\text{load}}}} \tag{3}$$

where T_0 is the instant where the transition occurs and R_X is the amplitude of the transient overcurrent for each phase. Said amplitude, given by (4), is calculated as the difference between the output current generated by the voltage waveforms associated to both modulation techniques at the instant of the transition between modulations. It takes this form due to the

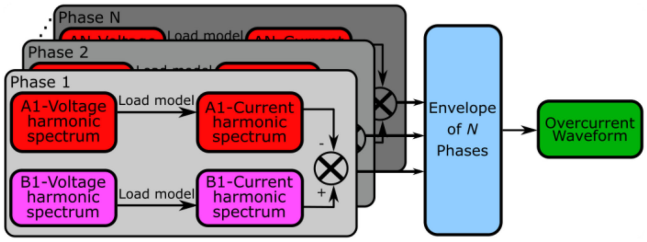

Fig. 2. Overcurrent waveform calculation process for *N*-phase systems.

inductive–resistive [L_{load} and R_{load}, respectively, in (3)] nature of the considered loads, i.e., asynchronous motors and permanent-magnet synchronous machines. Equation (4) provides an analytical expression to calculate the overcurrent in each phase. The transition time T_0 to minimize the overcurrent can then be calculated. However, this implies dealing with the addition of multiple harmonics that makes its interpretation and mathematical manipulation quite complex. Besides, all phases should be considered simultaneously for the calculation of T_0. Due to these facts, it is convenient to develop a numerical overcurrent minimization algorithm to calculate T_0.

III. Proposed Overcurrent Minimization Algorithm

The proposed offline overcurrent minimization algorithm is split into the following three steps.

1) First step evaluates the maximum overcurrent in any of the output phases when there is a transition between two modulation techniques.
2) Second, the dependencies of overcurrent with the electric parameters are determined.
3) Finally, the required T_0 to minimize the overcurrent is assessed. Issues regarding practical implementation are also addressed in this step.

Note that the proposed method is based on how to calculate the optimal time instant in order to execute the change from one given modulation scheme to another. The voltage and frequency where this transition needs to be done are assumed to be already evaluated as in [14]–[16].

A. Overcurrent Calculation Algorithm for the Modulation Transition

The process to calculate the overcurrent is represented in Fig. 2. First, the voltage amplitude, fundamental frequency, and modulation index at which the transition between modulations will take place need to be set. Once defined, the voltage waveforms for Modulation A and B for one fundamental period are obtained and their harmonic decomposition is calculated. Note that the main inputs used in the calculation are the harmonic components of the voltage waveforms. These can be obtained directly in the frequency domain (regardless of modulation technique) or calculated through a time-domain waveform.

Once both voltage waveforms are generated and their harmonic components are calculated, a load model that accurately represents the load behavior needs to be defined. With that purpose, an impedance frequency model is created, setting different impedances for each harmonic of the fundamental output frequency [32]. This model has different impedance formulation depending on the frequency as follows.

1) At the fundamental frequency, the operating current, voltage, and power factor are used to define the impedance value.
2) Higher order harmonics are modeled applying an impedance that is equal to the leakage inductances of the connected motor.

Then, having the voltage waveforms and the load model expressed in the frequency domain, the currents associated to each voltage waveform are obtained, so that the following equation can be calculated:

$$R_X\ (T_0) = \sum_{h=i}^{j} \left[\frac{V_{B,h}}{Z_h} \sin\left(h\omega T_0 + \gamma + \varphi_{B,h} + \theta_h\right) - \frac{V_{A,h}}{Z_h} \sin\left(h\omega T_0 + \gamma + \varphi_{A,h} + \theta_h\right) \right]. \quad (4)$$

Two different cases are considered as follows:

1) transition from an SHE pattern to another one with different number of angles;
2) transition from SVM to SHE, or vice versa.

Even though the scenario presented in Fig. 1 and (4) can be applied to both cases to calculate the overcurrent, each of them presents some singularities that must be taken into consideration. Results for both cases are shown in Fig. 3. Fig. 3(a) shows SVM to SHE11 transition, Fig. 3(b) and (c) shows SHE to SHE transitions, and, finally, Fig. 3(d) shows the SVM to SHE7

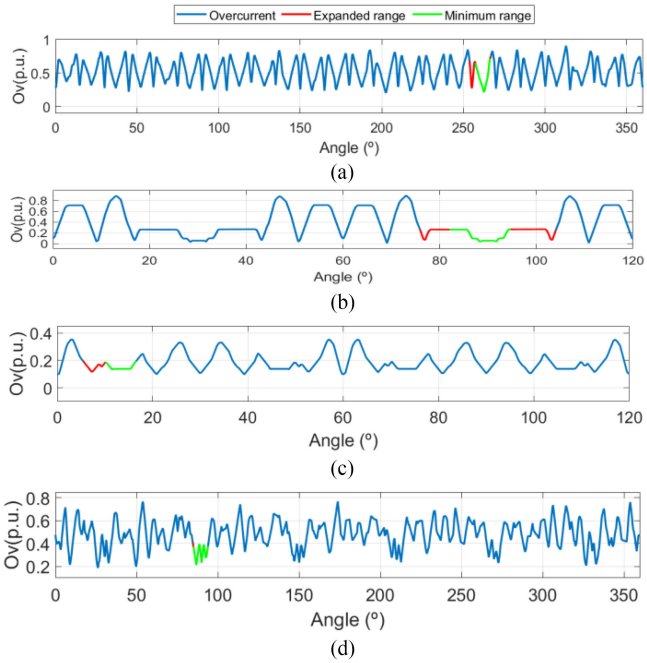

Fig. 3. Transition ranges for minimum overcurrent for the analyzed three-phase system. (a) SVM to SHE11 transition at 14 Hz, (b) SHE11 to SHE9 transition at 20 Hz, (c) SHE9 to SHE7 transition at 38 Hz, and (d) SVM to SHE7 transition at 14 Hz.

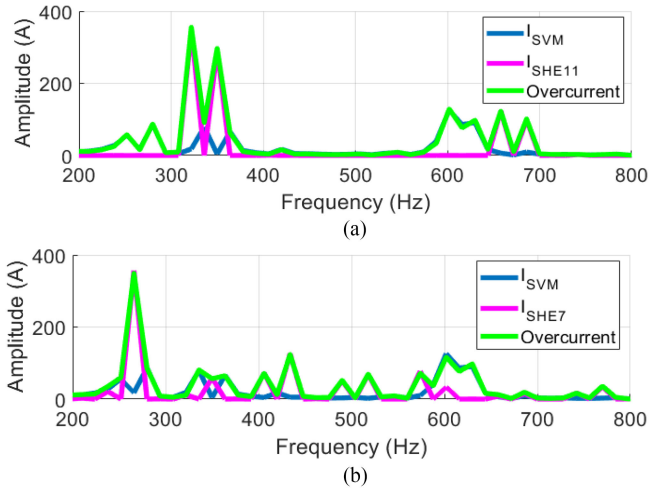

Fig. 4. Low harmonic spectrum of the currents and overcurrent at the SVM to SHE transition. (a) SVM to SHE11 strong influence of the 23rd and 25th harmonics and (b) SVM to SHE7 weaker harmonic influence.

transition to prove how the noneliminated current harmonics influence the resulting overcurrent waveform.

1) Transition Between Different SHEs: SHE is a synchronous modulation strategy in the sense that the amplitude and phase of the generated voltage harmonics are univocally defined and are independent of the fundamental frequency. Consequently, (4) can be unambiguously determined regardless the time instant when the transition between the modulations takes place and the value of the fundamental frequency.

Therefore, to determine the maximum transient overcurrent, calculation of $R_X(t)$ according to (4) for any time instant t within a fundamental period is made for all the phases of the converter.

As a case study, a three-phase system is considered, where $X = \{U,V,W\}$. Then, their absolute values are taken and the maximum one is selected.

Fig. 3(b) shows the maximum overcurrent amplitude when a transition from SHE11 to SHE 9 takes place at any time instant within a fundamental period (where the number of SHE means the number of angles in the first quarter of period). As it can be observed, there is a repeatability of 60° in the overcurrent pattern, which can be explained since the positive and negative half-periods of the same phase create the same absolute value of the overcurrent. This means that when a transition among two SHE patterns is performed, the optimum time instants with minimum overcurrent are found every sixth of the fundamental period.

2) Transition Between SVM and SHE: A similar approach can be followed to analyze the transition between SVM and SHE. For the sake of simplicity, SVPWM is considered in this article as a particularization of SVM. This assumption is made as its performance and harmonic spectrum can be considered similar to those of the SVM digital implementation [33]–[35]. The objective is to achieve voltage harmonic magnitudes and phases as given in (1).

When variable speed drives are considered, SVPWM behaves as an asynchronous modulation. The noninteger ratio between the switching and the fundamental frequency affects the symmetry of the voltage signals resulting in different voltage waveforms in every fundamental period. Due to this fact, it is necessary to consider the phase shift between the modulation and carrier signals to determine the harmonics of the voltage waveforms that define the overcurrent. Depending on the phase shift, the maximum and minimum overcurrents will take different values and will be generated at different time intervals. Therefore, to consider this uncertainty in the calculation algorithm, a parametric sweep of the phase shift from 0° to 360° is performed and a global overcurrent waveform is defined as the envelope (maximum) of the individual overcurrent waveforms of each considered phase shift. This way, a worst case scenario analysis is performed which guarantees that the maximum overcurrent will be always equal or smaller than that provided by the algorithm.

Unlike the previous case, the periodicity of the overcurrent cannot be generally assessed for the transition between SVM and SHE. It depends on the switching frequency of SVM and the number of angles of SHE. Fig. 4 shows the current spectrum of two possible SVM to SHE transitions. According to (4), the dominant harmonics of the overcurrent waveform that define its periodicity will be those that are not mutually canceled between the two modulation strategies. Fig. 4 illustrates that the first noncanceled predominant harmonics are different in both cases. Consequently, the periodicity of the overcurrent waveform is not the same.

B. Input Parameter Dependence

The overcurrent directly depends on the operating point where the converter performs the modulation transition. This operating point is defined by different parameters defined as follows:

1) dc bus voltage ($V_{\rm dc}$);
2) rated output voltage ($V_{\rm LLrms}$);
3) rated output frequency (f_o);
4) SHE patterns;
5) switching frequency if SVM;
6) control task time;
7) transition operating points (voltages and frequencies);
8) power factor of the load at the transition;
9) amplitude of the output current at the transition;
10) load parameters (leakage inductances, etc.).

The first seven parameters are predefined by the used converter, and completely define the synthesized output voltage that is needed to obtain the currents. The last three parameters are defined by the load and will determine the magnitude of the overcurrent; although the exact value of those parameters might not be available.

Due to this fact, the load parameter dependence of the overcurrent is analyzed by means of a parametric analysis of these three parameters, as illustrated in Fig. 5. The horizontal axis represents the phase angle of the first output phase that can be translated to time depending on the output fundamental frequency. The vertical axis represents the overcurrent waveform obtained considering the three-phase system, since one output phase might be near the zero crossing point, whereas the others have high current values.

The effect of the power factor of the load in the overcurrent is analyzed in Fig. 5(a). It is observed that the power factor does

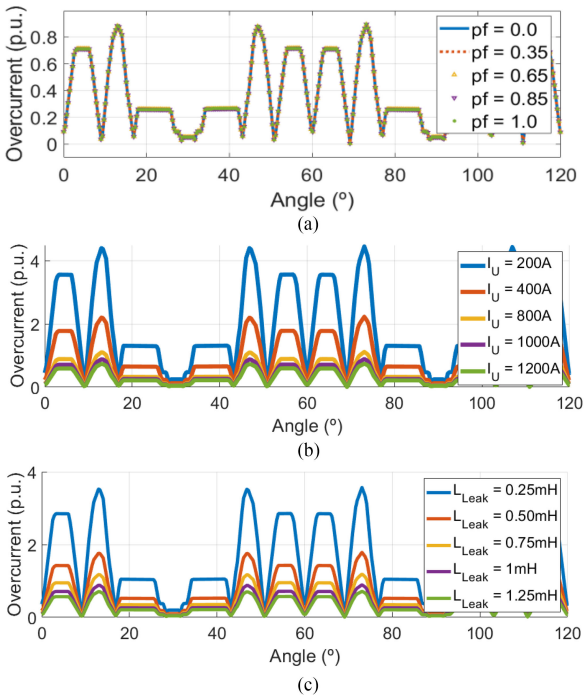

Fig. 5. Overcurrent at the transition from SHE11 to SHE9, output frequency 20 Hz. (a) Power factor where $I_{\text{base}} = 1000$ A, (b) rms value of the output current where $I_{\text{base}} = I_U$, and (c) rotor and stator leakage inductances where $I_{\text{base}} = 1000$ A.

not modify the overcurrent. This is explained since the power factor only affects the angle of fundamental voltage and current; the harmonics maintain the phase whichever the power factor is. Therefore, according to (4), the overcurrent is not affected. Hence, all the power factor plots in Fig. 5(a) are overlapped.

Fig. 5(b) shows the variation of the normalized overcurrent (overcurrent/amplitude of the fundamental) as the fundamental current changes. As expected from (4), the same overcurrent is generated regardless of the amplitude of the fundamental output current. Besides, the periods of time during which the overcurrent is minimum remain the same inside the fundamental period. Consequently, it is not necessary to take into account the amplitude of the fundamental output current for the calculation of the optimum transition time between modulations.

Finally, the impact of the total leakage inductance of the motor is analyzed in Fig. 5(c). Decreasing the leakage inductance results in a greater current ripple, while increasing it reduces the current ripple. Therefore, for the same fundamental output current, higher overcurrent is expected when the total leakage inductance is smaller. However, the overcurrent maximum and minimum points remain located at the same time instants.

C. Overcurrent Minimization Algorithm

The previous analysis has shown that the load power factor, the amplitude of the output current, and the leakage inductance can be neglected to calculate the time instant when the transition between modulations should take place to minimize the overcurrent. This simplification reduces the calculation complexity.

Utilizing the methodology described in Section III-A, the proposed overcurrent minimization algorithm implements an offline calculation of the overcurrent, due to the modulation transition, throughout the fundamental period as depicted in Fig. 3. Through this calculation, the transition angle (equivalent to the transition time instant) that minimizes the overcurrent is obtained. However, due to real-time implementation constraints, there is a minimum sampling period that should be considered for the calculation of the transition angle that is defined by the control task period. The proposed algorithm needs to calculate a range of transition angles with a duration of at least one control task period. In this way, it is assured that there is always an optimum transition angle within a fundamental period at the sampling time period defined by the control task. Minimum integral average per control period (T_c) equation is defined in the following equation:

$$I_{AVE,Tc} = \sum_{i=1}^{M-N} \left[\frac{\Delta Ov\,(i) \cdot \Delta\varphi\,(i)}{2} \right] \tag{5}$$

where M is the total number of points used and N is the number of points for the sliding window. Minimum integral index $\boldsymbol{i}$ is saved, once the whole waveform has been analyzed. Additionally, ΔOv is the overcurrent variation [see (4)] inside the sliding window at the starting point i. $\Delta\varphi$ is the angle variation in a sliding window.

This is implemented applying a sliding window, whose width is equivalent to a control task period, over the overcurrent calculated previously (see Fig. 3). The selected range of optimum angles is defined so that it provides the minimum average overcurrent value over the sliding window. In addition, if surrounding angles provide less overcurrent than the average value, the optimum angle range is expanded to include these angles. Fig. 3 illustrates in blue the overcurrent along the fundamental period, the minimum range found is plotted in green, and the expanded range is plotted in red. The figure evaluates the transition for different modulation techniques and operating points, which could be an example of an acceleration switching pattern in a real power converter.

IV. Simulation Results

A. Case Study

A three-level (3L) neutral–point-clamped (NPC) [7]–[9] converter is simulated using the scheme of Fig. 6, where instead of capacitors, dc sources simulate an ideal dc bus; this means that the floating neutral point (0 in Fig. 6) is always balanced. In this way, there will be no unbalanced neutral floating point that affects the results.

The case study presented in this article represents a 3L NPC drive that, without a proper modulation transition management, can register serious overcurrent during its operation, resulting in emergency stops of the converter.

The operating conditions and modulation characteristics are summarized in Table I . The proposed methodology is applied to three different transitions: SVM to SHE11, SHE11 to SHE9, and SHE9 to SHE7. Their respective transition frequencies are

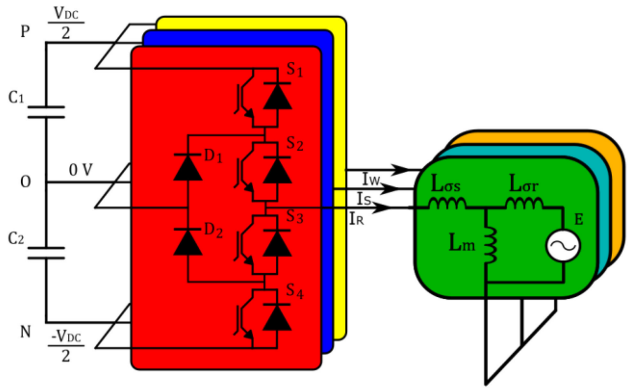

Fig. 6. 3L NPC voltage source converter connected to an inductive–resistive load.

TABLE I
CASE STUDY PARAMETERS

Control frequency, f_c	2444 Hz
Switching frequency (SVM), fs	305.5 Hz
Transition frequencies	14 Hz – 20 Hz – 38 Hz
DC bus, V_{dc}	5100 V
Motor voltage, V_{motor}	3300 V
Motor current, I_{motor}	1354 A
Motor power, P_{motor}	6500 kW
Frequency, f_{nom}	50 Hz

TABLE II
SHE TABLES AND TRANSITION FREQUENCIES

Converter	1st Transition	2nd Transition	3rd Transition
Case Study	SHE11 – 14 Hz	SHE9 – 20 Hz	SHE7 – 38 Hz

TABLE III
ANGLE RANGES FOR OPTIMUM MODULATION TRANSITIONS

Converter	Range0 (°)	Range1 (°)	Range2 (°)
Case Study	[253.80 – 266.76]	[15.96 – 44.04]	[5.40 – 16.56]

displayed in Table II. Note that for different converter implementations, the SVM switching frequency may vary, along with the control task period. Therefore, different widths for the optimum angle range should be considered.

The results obtained with the proposed algorithm are shown in Table III, where Range0, Range1, and Range2 are the optimum transition angle ranges found for SVM to SHE11, SHE11 to SHE9, and SHE9 to SHE7 transitions, respectively. Note that these results are specific of the set of SHE firing angles used. Therefore, different sets of firing angles for the same operating conditions [20] will result in different optimum angle ranges.

A further study of the transitions is conducted at different modulation indices (and frequencies considering a *V/f* control).

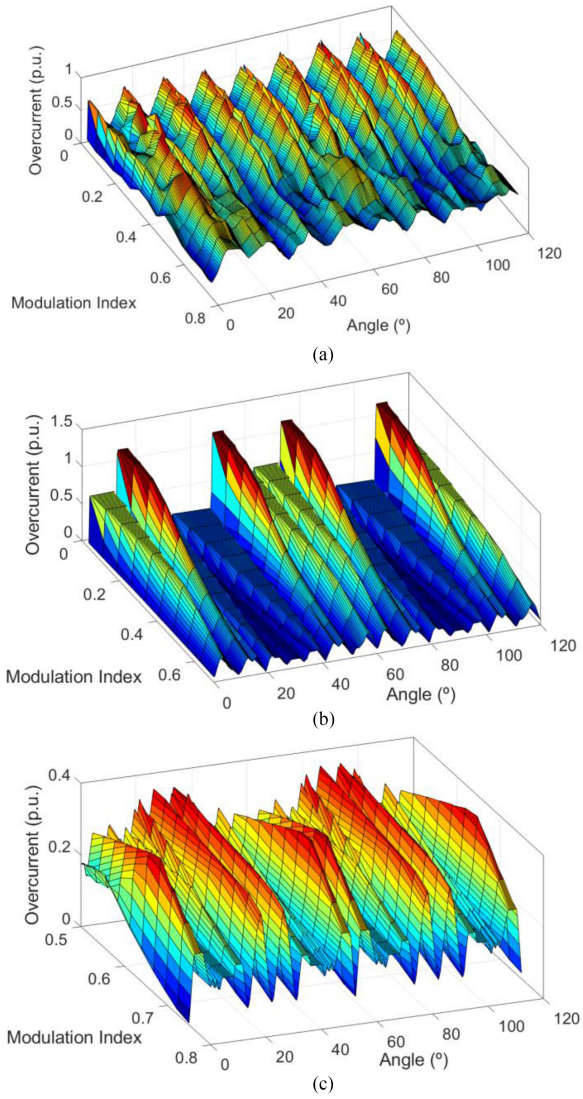

Fig. 7. Transition evaluation at different operating points. (a) SVM to SHE11 transition. (b) SHE11 to SHE9 transition. (c) SHE9 to SHE7 transition.

Fig. 7 shows how the normalized overcurrent changes as the modulation index increases for the transitions among SVM to SHE11, SHE11 to SHE9, and SHE9 to SHE7, respectively.

Transition angles are represented between 0° and 120° for the SHE cases, although they can be replicated up to six times in the same fundamental period. This is due to the fact that between some SHE tables, the optimum range is centered at 60°.

As seen in Fig. 7(b) and (c), when SHE transitions are considered, the minimum overcurrent angle remains constant for every modulation index.

In Fig. 7(a), a similar behavior is observed, although variations can be noticed due to the changes in the carrier to output frequency ratio, as it has been explained in Section III-B. Consequently, in the case of SHE to SHE transitions, the frequency and modulation index can change while the optimum transition angle will remain constant. This fact is true in case of SVM to SHE transitions, when just small variations of frequency and modulation index are regarded.

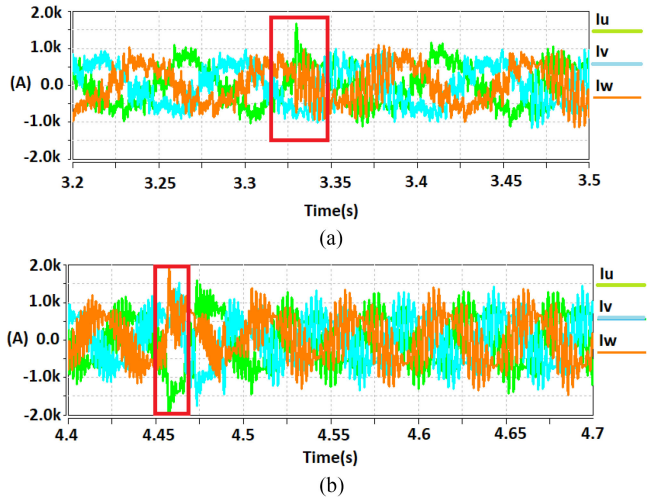

Fig. 8. MV drive simulation. (a) Overcurrent in the SVM to SHE11 transition at 14 Hz and (b) overcurrent in the SHE11 to SHE9 transition at 20 Hz.

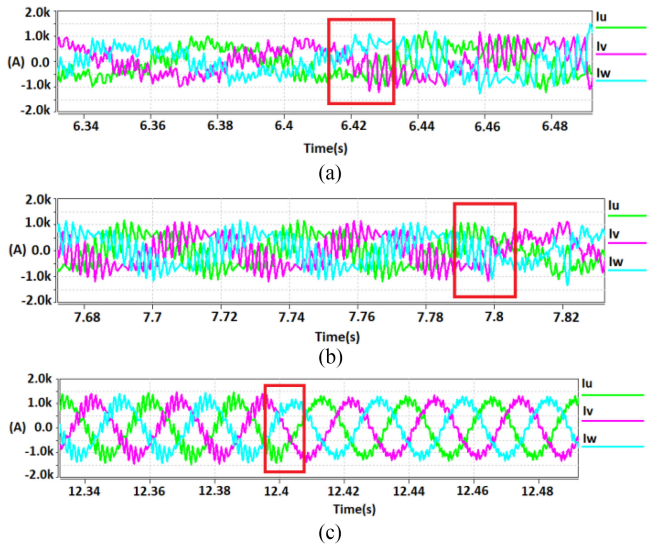

Fig. 9. MV drive simulation applying the transition control algorithm. (a) SVM to SHE11 transition. (b) SHE11 to SHE9 transition. (c) SHE9 to SHE7 transition.

B. Transition Control Algorithm Simulation

Figs. 8 and 9 show electromagnetic transient simulations when a 3L NPC drive, using the data from in Table I, is operated without and with the proposed modulation transition management, respectively. In Fig. 8(a), a transition between SVM and SHE11 takes place, which produces a transient overcurrent that, despite considerable, it is not large enough to surpass the overcurrent converter limits. Fig. 8(b) shows a transition between SHE11 and SHE9, which produces a considerable transient overcurrent as well. In this case, the overcurrent peak surpasses the overcurrent protection limit set for the converter. In a real converter, this issue may imply a complete emergency shut down of the converter.

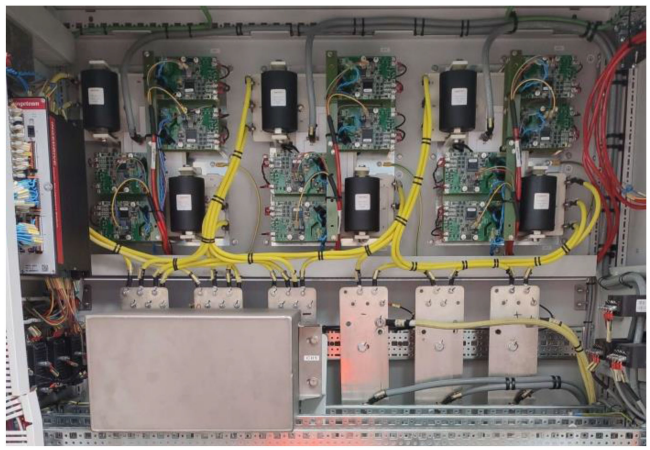

Fig. 10. Experimental scaled-down converter.

TABLE IV
SCALED-DOWN EQUIPMENT PARAMETERS

Control frequency, fc	2444 Hz
Switching frequency (SVM), fs	1222 Hz
SHE families	SHE11 – SHE9 – SHE7
Transition frequencies	20 Hz – 38 Hz – 43 Hz
DC-link voltage, V_{dc}	430 V
Motor voltage, V_{motor}	400 V
Motor current, I_{motor}	67 A
Motor power, P_{motor}	45 kW
Nominal frequency, f_{nom}	50 Hz

These results confirm that serious overcurrent might happen when changing the modulation technique on variable speed drive applications.

Fig. 9 shows the current waveforms during transitions from SVM to SHE11, SHE11 to SHE9, and SHE9 to SHE7. These results are obtained under the same previous working conditions, but when the transition between modulations is performed at the optimum time instant according to the proposed algorithm. In all the three cases, the transient overcurrent is minimized, proving the ability of the proposed modulation transition algorithm to determine the optimum time instant and to minimize the transient overcurrent.

V. EXPERIMENTAL RESULTS

A. Scaled-Down Converter

In order to completely validate the proposed method, an experiment is conducted using a scaled-down converter (see Fig. 10 and parameters in Table IV). In the next section, the algorithm is applied to the actual MV converter from Table I, showing how critic it can be in demanding applications.

The optimum transition ranges are calculated and applied in the same way as in Section IV. First, the converter implements the modulation transition at a nonoptimal instant that produces a significant overcurrent (see Fig. 11). Several signals are represented; V_u and I_u are the oscilloscope measured output

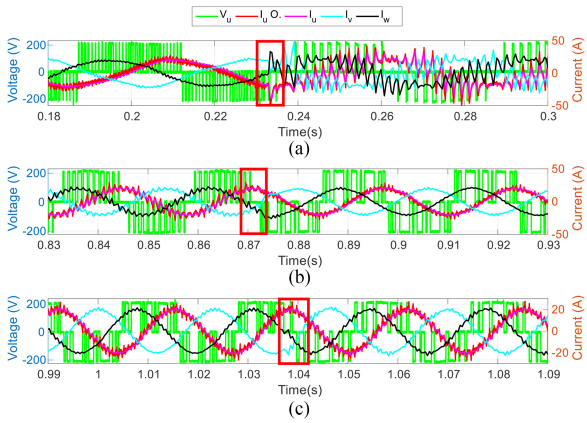

Fig. 11. Scaled-down experimental results without applying the transition control algorithm. (a) SVM to SHE11 transition at 20 Hz. (b) SHE11 to SHE9 transition at 38 Hz. (c) SHE9 to SHE7 transition at 43 Hz.

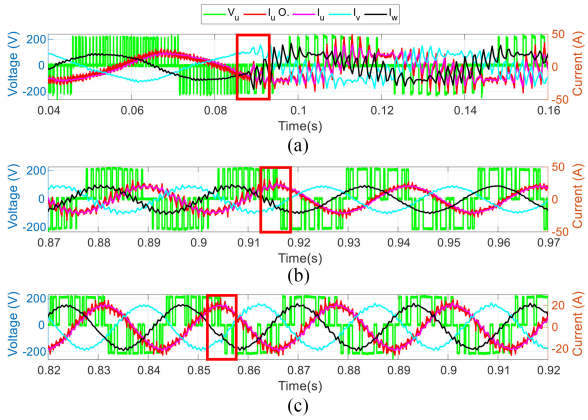

Fig. 12. Scaled-down experimental results applying the transition control algorithm. (a) SVM to SHE11 transition at 20 Hz. (b) SHE11 to SHE9 transition at 38 Hz. (c) SHE9 to SHE7 transition at 43 Hz.

voltage and current of phase U of the converter, respectively; I_v and I_w are, respectively, the currents of phases V and W registered and filtered by the controller. As it can be noticed, the ripple of these currents is slightly attenuated due to the filter, resulting in lower measured overcurrent.

In Fig. 11(a), an overcurrent takes place when SVM is replaced by SHE11 in phase U. In Fig. 11(b) and (c), the overcurrent takes place in phases V and W. The peaks are clearly observed, even though just the filtered signals are displayed, which provides lower overcurrent values than real ones.

In Fig. 12, the optimal transition angles are applied. Comparing to Fig. 11, the transient overcurrent during the modulation transitions is greatly reduced. In this way, the maximum ratings of the converter are never exceeded.

B. Medium-Voltage Converter

Field results were also obtained for the MV drive described and modeled in Section IV (see Fig. 13 and parameters in Table I). These results, obtained from a full-scale commercial

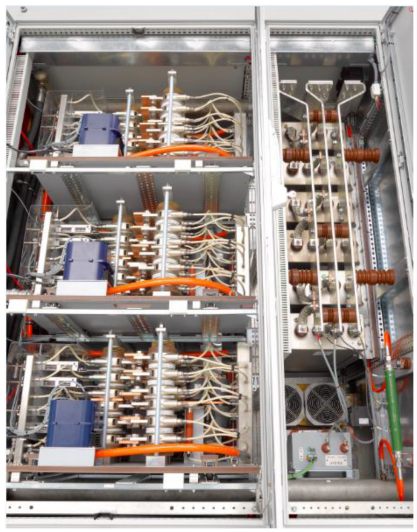

Fig. 13. Ingedrive MV500 3L NPC full-scale converter.

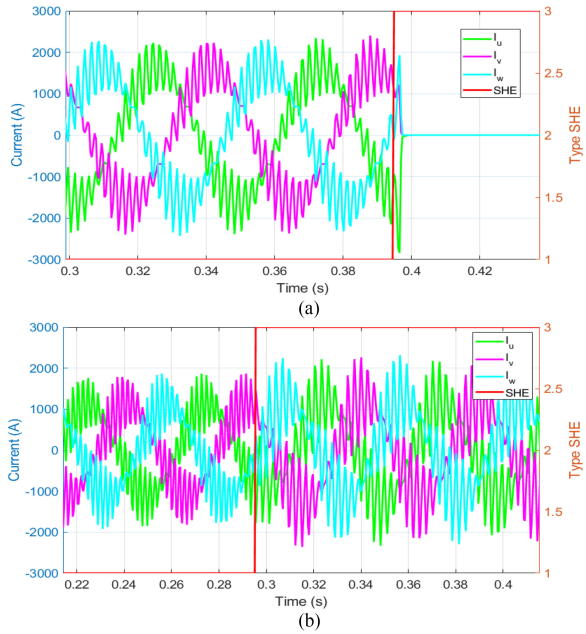

Fig. 14. SHE11 to SHE9 transition on a real MV drive at 20 Hz. (a) Transition without algorithm. (b) Transition applying the algorithm.

power converter working in a real mining application, complement the experimental results obtained from the scaled-down converter of Section IV-A.

Results are much more visual on the Ingedrive MV500 than in the laboratory scaled-down equipment. This is due to the smaller inductance of the MV motor connected to the drive. As it can be noticed in Fig. 14(a), if the modulation transition is not controlled by the proposed algorithm, it produces an overcurrent (2840 A) that surpasses the converter current ratings, resulting in an emergency stop, making it impossible to further increase the output frequency, thus, no registers could be obtained to show the transition without the overcurrent minimization algorithm.

However, in Fig. 14 (b) the transition algorithm is applied and no overcurrent takes place, ensuring the safe operation of

the drive. If Figs. 8 and 14 are compared, a difference in the current amplitude can be noticed from the simulation to the real application. The simulation results were performed with no load, due to the uncertainty of the load (active power and power factor values) of the application. However, as explained in Section III-B, the optimal transition range is independent of the power factor and current amplitude. These results demonstrate the suitability of the proposed method in a real application.

VI. Conclusion

This article has presented a mathematical analysis and a method to minimize the transient overcurrent in variable speed drives when there is a transition between different modulations. It provides the optimum angle (time instant) when the transition should take place to minimize the overcurrent. Besides, the dependence of the transient overcurrent on different converter and load parameters has been analyzed as well, improving the applicability of the proposed method to a real converter.

The method has been successfully proven in a 3L NPC drive with different modulation transitions, i.e., SVM to SHE or SHE to SHE with different number of firing angles. However, it is general and can be applied to any converter topology and modulation technique.

Simulation and experimental results illustrate the effectiveness of the proposed method to limit the modulation transition overcurrent.

References

[1] B. Wu, *High-Power Converters and AC Drives*. Hoboken, NJ, USA: Wiley, 2010.

[2] A. Sanchez-Ruiz, M. Mazuela, S. Alvarez, G. Abad, and I. Baraia, "Medium voltage–high power converter topologies comparison procedure, for a 6.6 kV drive application using 4.5 kV IGBT modules," *IEEE Trans. Ind. Electron.*, vol. 59, no. 3, pp. 1462–1476, Mar. 2012.

[3] M. A. Perez, S. Bernet, J. Rodriguez, S. Kouro, and R. Lizana, "Circuit topologies, modeling, control schemes, and applications of modular multilevel converters," *IEEE Trans. Power Electron.*, vol. 30, no. 1, pp. 4–17, Jan. 2015.

[4] J. Rodriguez, J.-S. Lai, and F. Z. Peng, "Multilevel inverters: A survey of topologies, controls, and applications," *IEEE Trans. Ind. Electron.*, vol. 49, no. 4, pp. 724–738, Aug. 2002.

[5] D. G. Holmes and T. A. Lipo, *Pulse Width Modulation for Power Converters Principles and Practice*. Hoboken, NJ, USA: Wiley, 2003.

[6] J. I. Leon, S. Kouro, L. G. Franquelo, J. Rodriguez, and B. Wu, "The essential role and the continuous evolution of modulation techniques for voltage-source inverters in the past, present, and future power electronics," *IEEE Trans. Ind. Electron.*, vol. 63, no. 5, pp. 2688–2701, May 2016.

[7] S. Kouro, J. Rodriguez, B. Wu, S. Bernet, and M. Perez, "Powering the future of industry: High-power adjustable speed drive topologies," *IEEE Ind. Appl. Mag.*, vol. 18, no. 4, pp. 26–39, Jul. 2012.

[8] J. Rodriguez, S. Bernet, B. Wu, J. O. Pontt, and S. Kouro, "Multilevel voltage-source-converter topologies for industrial medium-voltage drives," *IEEE Trans. Ind. Electron.*, vol. 54, no. 6, pp. 2930–2945, Dec. 2007.

[9] J. Rodriguez, S. Bernet, P. K. Steimer, and I. E. Lizama, "A survey on neutral-point-clamped inverters," *IEEE Trans. Ind. Electron.*, vol. 57, no. 7, pp. 2219–2230, Jul. 2010.

[10] G. Alonso Orcajo *et al.*, "Retrofit of a hot rolling mill plant with three-level active front end drives," *IEEE Trans. Ind. Appl.*, vol. 54, no. 3, pp. 2964–2974, May 2018.

[11] B. P. Schmitt and R. Sommer, "Retrofit of fixed speed induction motors with medium voltage drive converters using NPC three-level inverter high-voltage IGBT based topology," in *Proc. IEEE Int. Symp. Ind. Electron. Proc.*, Jun. 2001, vol. 2, pp. 746–751.

[12] S. Bernet, "Recent developments of high power converters for industry and traction applications," *IEEE Trans. Power Electron.*, vol. 15, no. 6, pp. 1102–1117, Nov. 2000.

[13] S. Kouro *et al.*, "Recent advances and industrial applications of multilevel converters," *IEEE Trans. Ind. Electron.*, vol. 57, no. 8, pp. 2553–2580, Aug. 2010.

[14] A. Sanchez-Ruiz, G. Abad, S. Alvarez, and L. M. Tolbert, "Modulation selection procedure applied to a high-power adjustable high-speed drive," in *Proc. 15th Eur. Conf. Power Electron. Appl.*, Sep. 2013, pp. 1–10.

[15] M. Steczek, P. Chudzik, and A. Szelag, "Combination of SHE- and SHM-PWM techniques for VSI DC-Link current harmonics control in railway applications," *IEEE Trans. Ind. Electron.*, vol. 64, no. 10, pp. 7666–7678, Oct. 2017.

[16] M. Mazuela, A. Sanchez-Ruiz, I. Echeverría, S. Telleria, and I. Atutxa, "Modulation and LCR filter optimum design procedure for medium voltage adjustable speed drives," in *Proc. 18th Eur. Conf. Power Electron. Appl.*, Sep. 2016, pp. 1–10.

[17] D. G. Holmes and B. P. McGrath, "Opportunities for harmonic cancellation with carrier-based PWM for a two-level and multilevel cascaded inverters," *IEEE Trans. Ind. Appl.*, vol. 37, no. 2, pp. 574–582, Mar. 2001.

[18] H. D. T. Mouton, B. McGrath, D. G. Holmes, and R. H. Wilkinson, "One-dimensional spectral analysis of complex PWM waveforms using superposition," *IEEE Trans. Power Electron.*, vol. 29, no. 12, pp. 6762–6778, Dec. 2014.

[19] B. P. McGrath, D. G. Holmes, and T. Lipo, "Optimized space vector switching sequences for multilevel inverters," *IEEE Trans. Power Electron.*, vol. 18, no. 6, pp. 1293–1301, Nov. 2003.

[20] M. S. A. Dahidah, G. Konstantinou, and V. G. Agelidis, "A review of multilevel selective harmonic elimination PWM: Formulations, solving algorithms, implementation and applications," *IEEE Trans. Power Electron.*, vol. 30, no. 8, pp. 4091–4106, Aug. 2015.

[21] J. Napoles, J. I. Leon, R. Portillo, L. G. Franquelo, and M. A. Aguirre, "Selective harmonic mitigation technique for high-power converters," *IEEE Trans. Ind. Electron.*, vol. 57, no. 7, pp. 2315–2323, Jul. 2010.

[22] A. Sanchez-Ruiz, G. Abad, I. Echeverria, I. Torre, and I. Atutxa, "Continuous phase-shifted selective harmonic elimination and DC-Link voltage balance solution for H-bridge multilevel configurations, applied to 5L HNPC," *IEEE Trans. Power Electron.*, vol. 32, no. 4, pp. 2533–2545, Apr. 2017.

[23] A. Perez-Basante *et al.*, "Circulating current control for modular multilevel converters with (N+1) selective harmonic Elimination—PWM," *IEEE Trans. Power Electron.*, vol. 35, no. 8, pp. 8712–8725, Aug. 2020.

[24] A. Perez-Basante, S. Ceballos, G. Konstantinou, J. Pou, I. Kortabarria, and I. M. de Alegria, "A universal formulation for multilevel selective-harmonic-eliminated PWM with half-wave symmetry," *IEEE Trans. Power Electron.*, vol. 34, no. 1, pp. 943–957, Jan. 2019.

[25] G. Konstantinou, M. Ciobotaru, and V. Agelidis, "Selective harmonic elimination pulse-width modulation of modular multilevel converters," *IET Power Electron.,* vol. 6, no. 1, pp. 96–107, Jan. 2013.

[26] T. Geyer, N. Oikonomou, G. Papafotiou, and F. Kieferndorf, "Model predictive pulse pattern control," *IEEE Trans. Ind. Appl.*, vol. 48, no. 2, pp. 663–676, Mar.–Apr. 2012.

[27] E. H. Aboadla *et al.*, "Effect of duty cycle on THD for multilevel inverter based on selective harmonic elimination technique," in *Proc. 7th Int. Conf. Comput. Commun. Eng.*, Sep. 2018, pp. 56–61.

[28] R. Alvarez, F. Filsecker, and S. Bernet, "Characterization of a new 4.5 kV press pack SPT+ IGBT for medium voltage converters," in *Proc. IEEE Energy Convers. Congr. Expo.*, Sep. 2009, pp. 3954–3962.

[29] S. Dieckerhoff, S. Bernet, and D. Krug, "Power loss-oriented evaluation of high voltage IGBTs and multilevel converters in transformerless traction applications," *IEEE Trans. Power Electron.*, vol. 20, no. 6, pp. 1328–1336, Nov. 2005.

[30] A. Wilson and S. Bernet, "Comparative evaluation of three-level converters using 4.5 kV, 1.2 kA IGBT modules," in *Proc. IEEE Int. Conf. Ind. Technol.*, Mar. 2015, pp. 3040–3045.

[31] S. Vazquez, J. I. Leon, L. G. Franquelo, J. J. Padilla, and J. M. Carrasco, "DC-voltage-ratio control strategy for multilevel cascaded converters fed with a single DC source," *IEEE Trans. Ind. Electron.*, vol. 56, no. 7, pp. 2513–2521, Jul. 2009.

[32] A. Sanchez-Ruiz, J. J. Valera, I. Legarra, I. Torre, S. Telleria, and I. Atutxa, "Modelling of MVDC multidrive systems for power quality analysis," in *IEEE Trans. Ind. Electron.*, to be published, doi: 10.1109/TIE.2020.2996143.

[33] A. M. Hava, R. J. Kerkman, and T. A. Lipo, "Simple analytical and graphical methods for carrier-based PWM-VSI drives," *IEEE Trans. Power Electron.*, vol. 14, no. 1, pp. 49–61, Jan. 1999.

[34] B. P. McGrath and D. G. Holmes, "An analytical technique for the determination of spectral components of multilevel carrier-based PWM methods," *IEEE Trans. Ind. Electron.*, vol. 49, no. 4, pp. 847–857, Aug. 2002.
[35] B. McGrath and H. d T. Mouton, "One-Dimensional spectral analysis techniques for multilevel PWM strategies," *IEEE Trans. Power Electron.*, vol. 31, no. 10, pp. 6910–6919, Oct. 2016.

Hector Fernandez-Rebolleda was born in Torrelavega, Spain, in 1995. He received the B.Sc. degree in industrial engineering and the M.Sc. degree in industrial engineering from the University of Cantabria, Santander, Spain, in 2017 and 2018, respectively, and the M.Sc. degree in industrial automation, electronics, and control from the University of Deusto, Bilbao, Spain, in 2019.

In February 2019, he joined Ingeteam Power Technology, Zamudio, Spain, where he is currently a Control and Regulation Engineer with the Department of Marine & Industry. His current research interests include modulation, control of power converters, multilevel topologies, advanced modulation techniques, and high-power motor drives.

Alain Sanchez-Ruiz (Senior Member, IEEE) received the B.Sc. degree in electronics engineering, the M.Sc. degree in automatics and industrial electronics, and the Ph.D. degree in electrical engineering from the University of Mondragon, Mondragon, Spain, in 2006, 2009, and 2014, respectively.

In May 2014, he joined Ingeteam R&D Europe, Zamudio, Spain, where he is currently an R&D Engineer. Since January 2017, he has also been a Lecturer with the University of the Basque Country (UPV/EHU), Bilbao, Spain. From February to May 2012, he was a Visiting Researcher with the University of Tennessee, Knoxville, TN, USA. His current research interests include modeling, modulation, and control of power converters, multilevel topologies, advanced modulation techniques, high-power motor drives, and grid-tied converters.

Salvador Ceballos received the M.S. degree in physics from the University of Cantabria, Santander, Spain, in 2001, and the M.S. and Ph.D. degrees in electronic engineering from the University of the Basque Country, Bilbao, Spain, in 2002 and 2008, respectively.

Since 2002, he has been with Tecnalia Research & Innovation, Derio, Spain, where he is currently a Principal Researcher in the Energy and Environment Division. His research interests include multilevel converters for high- and medium-voltage applications, fault-tolerant power electronic topologies, renewable energy systems, and power systems with high penetration of power converters.

Angel Perez-Basante received the B.Eng. degree in telecommunications engineering from the University of Valladolid, Valladolid, Spain, in 2006, the M.Eng. degree in electronic systems engineering from the Technical University of Madrid (UPM), Madrid, Spain, in 2012, and the Ph.D. degree in advanced electronic systems engineering from the University of the Basque Country (UPV/EHU), Bilbao, Spain, in 2017.

Since March 2017, he has been working as a Researcher with Tecnalia Research & Innovation in the Energy and Environment Division. From 2012 to 2016, he was a Ph.D. Student with the Applied Electronics Research Team (APERT), University of the Basque Country (UPV/EHU) in collaboration with Tecnalia Research & Innovation. From September to December 2015, he was a Visiting Researcher with the Chair of Power Electronics of the Christian Albrechts University, Kiel, Germany. His main research interests include multilevel converters, modulation and control strategies for MVdc/HVdc converters and renewable energy systems.

Juan José Valera-García was born in Bilbao, Spain, in 1970. He received the B.Eng. degree from Mondragon University, Mondragon, Spain, in 1993, the M.Sc. degree in electronics and control engineering from the University of the Basque Country, Bilbao, Spain, in 2008, and the Ph.D. degree in control engineering, automation, and robotics from the University of the Basque Country, Bilbao, Spain, in 2013.

From 1995 to 2008, he was with Ingeteam as a Control Engineer for the industry and marine sectors. From 2008 to 2012, he was a Senior Researcher with Tecnalia Research & Innovation Center (Spain) working in projects related to drive control systems for electric and hybrid vehicles. In 2012, he came back to Ingeteam R&D Europe to work on R&D projects related to electric and hybrid propulsion systems and drives for industry and marine sectors. From 2012, he has been a Lecturer with the Control Engineering Department, University of the Basque Country. He has authored or coauthored several research and technical papers in the fields of electric and hybrid vehicles, energy management systems, control of power systems, control engineering, and intelligent control.

Georgios Konstantinou (Senior Member, IEEE) received the B.Eng. degree in electrical and computer engineering from the Aristotle University of Thessaloniki, Thessaloniki, Greece, in 2007, and the Ph.D. degree in electrical engineering from The University of New South Wales (UNSW) Sydney, Sydney, NSW, Australia, in 2012.

From 2013 to 2016, he was a Senior Research Associate with the UNSW Sydney, where he was part of the Australian Energy Research Institute. Since 2017, he has been with the School of Electrical Engineering and Telecommunications, UNSW Sydney, where he is currently a Senior Lecturer. His main research interests include multilevel converters, power electronics in HVdc, renewable energy, and energy storage applications.

Dr. Konstantinou is an Associate Editor for the IEEE TRANSACTIONS ON POWER ELECTRONICS, IEEE TRANSACTIONS ON INDUSTRIAL ELECTRONICS, and *IET Power Electronics*.

Josep Pou (Fellow, IEEE) received the B.S., M.S., and Ph.D. degrees in electrical engineering from the Technical University of Catalonia (UPC)—Barcelona Tech, Barcelona, Spain, in 1989, 1996, and 2002, respectively.

In 1990, he joined the Faculty of UPC as an Assistant Professor, where he became an Associate Professor in 1993. From February 2013 to August 2016, he was a Professor with the University of New South Wales (UNSW) Sydney, Sydney, NSW, Australia. He is currently a Professor with the Nanyang Technological University (NTU), Singapore, where he is the Program Director of Power Electronics at the Energy Research Institute at NTU (ERI@N) and the Co-Director of the Rolls-Royce at NTU Corporate Lab. From February 2001 to January 2002, and then February 2005 to January 2006, he was a Researcher with the Center for Power Electronics Systems, Virginia Tech, Blacksburg, VA, USA. From January 2012 to January 2013, he was a Visiting Professor with the Australian Energy Research Institute, UNSW Sydney. He has authored more than 350 technical papers and has been involved in several industrial projects and educational programs in the fields of power electronics and systems. His research interests include modulation and control of power converters, multilevel converters, renewable energy, energy storage, power quality, HVdc transmission systems, and more-electrical aircraft and vessels.

Dr. Pou is currently an Associate Editor for the IEEE JOURNAL OF EMERGING AND SELECTED TOPICS IN POWER ELECTRONICS. He was the Co-Editor-in-Chief and Associate Editor for the IEEE TRANSACTIONS ON INDUSTRIAL ELECTRONICS. He was the recipient of the 2018 IEEE Bimal Bose Award for Industrial Electronics Applications in Energy Systems.